Geophysical Research Letters®

Key Points:

- We develop analytical solutions for gravity changes due to the point Compound Dislocation Model simulating triaxial expansions
- Rapid coupled inversions of deformation and gravity changes, accounting for deformation-induced gravity changes are now possible
- For shallow sources, estimation errors in the chamber volume change may lead to large biases in the simulated gravity changes

Correspondence to:

M. Nikkhoo and E. Rivalta,
mehdi.nikkhoo@gfz-potsdam.de;
eleonora.rivalta@unibo.it

Author Contributions:

Conceptualization: Mehdi Nikkhoo, Eleonora Rivalta
Formal analysis: Mehdi Nikkhoo
Funding acquisition: Eleonora Rivalta
Investigation: Mehdi Nikkhoo, Eleonora Rivalta
Methodology: Mehdi Nikkhoo, Eleonora Rivalta
Project Administration: Mehdi Nikkhoo, Eleonora Rivalta
Resources: Mehdi Nikkhoo, Eleonora Rivalta
Software: Mehdi Nikkhoo
Supervision: Eleonora Rivalta
Validation: Mehdi Nikkhoo
Visualization: Mehdi Nikkhoo
Writing – original draft: Mehdi Nikkhoo, Eleonora Rivalta
Writing – review & editing: Mehdi Nikkhoo, Eleonora Rivalta

Analytical Solutions for Gravity Changes Caused by Triaxial Volumetric Sources

Mehdi Nikkhoo[1] and **Eleonora Rivalta[1,2]**

[1]GFZ German Research Centre for Geosciences, Potsdam, Germany, [2]Department of Physics and Astronomy, Alma Mater Studiorum University of Bologna, Bologna, Italy

Abstract Volcanic crises are often associated with magmatic intrusions or the pressurization of magma chambers of various shapes. These volumetric sources deform the country rocks, changing their density, and cause surface uplift. Both the net mass of intruding magmatic fluids and these deformation effects contribute to surface gravity changes. Thus, to estimate the intrusion mass from gravity changes, the deformation effects must be accounted for. We develop analytical solutions and computer codes for the gravity changes caused by triaxial sources of expansion. This establishes coupled solutions for joint inversions of deformation and gravity changes. Such inversions can constrain both the intrusion mass and the deformation source parameters more accurately.

Plain Language Summary Volcanic crises are usually associated with magmatic fluids that intrude and deform the host rocks before potentially breaching the Earth's surface. It is important to estimate how much fluid (mass and volume) is on the move. Volume can be determined from the measured surface uplift. Mass can be determined from surface gravity changes. The fluid intrusion increases the mass below the volcano, thereby increasing the gravity and pressurizing the rocks. This dilates parts of the host rock and compresses other parts, changing the rock density and redistributing the rock mass. This causes secondary gravity changes, called deformation-induced gravity changes. The measured gravity change is always the sum of the mass and deformation-induced contributions. Here, we develop mathematical equations for the rapid estimation of these deformation-induced gravity changes caused by arbitrary intrusion shapes. This way we can take the mass contribution apart from the deformation contribution. We show that by using this solution not only the intrusion mass, but also other intrusion parameters, including the volume, depth, and shape can be calculated more accurately.

1. Introduction

Intrusion of magma through the host rock or into an existing magma chamber deforms the Earth's crust and also changes the surface gravity field. The intrusion mass is a key parameter for characterizing the nature of the activity and its future evolution. Joint analyses of the measured surface displacements and gravity changes can constrain the intrusion mass, beside the other parameters of the deformation source, that is, its location, shape, spatial orientation, and some strength parameter (pressure or volume change; Battaglia et al., 1999, 2003; Okubo et al., 1991).

Both the mass transport and the ensuing country-rock deformations contribute to the gravity changes (Bonafede & Mazzanti, 1998; Hagiwara, 1977; Lisowski, 2007; Walsh & Rice, 1979). Such deformation-induced effects may be substantial for nonspherical sources, as shown through numerical models based on the finite element method (FEM; see Currenti, 2014; Currenti et al., 2007, 2008; Trasatti & Bonafede, 2008). The deformation effects caused by tabular sources such as dikes and sills can be estimated through the Okubo (1992) analytical solutions. There are no analytical solutions for other source geometries, such as ellipsoids, yet rigorous joint inversions of surface displacements and gravity changes demand models accounting for the source shape (Amoruso et al., 2008).

A source model composed of three orthogonal tensile dislocations can simulate the deformation field associated with triaxial sources (Amoruso & Crescentini, 2013; Bonafede & Ferrari, 2009; Lisowski et al., 2008). Based on this concept, Nikkhoo et al. (2017) developed the point Compound Dislocation Model (point CDM), which represents the far-field deformation of generic triaxial sources. This source model spans a wider parameter space than ellipsoids (Ferrari et al., 2015) while retaining the simplicity of the Mogi (1958) model.
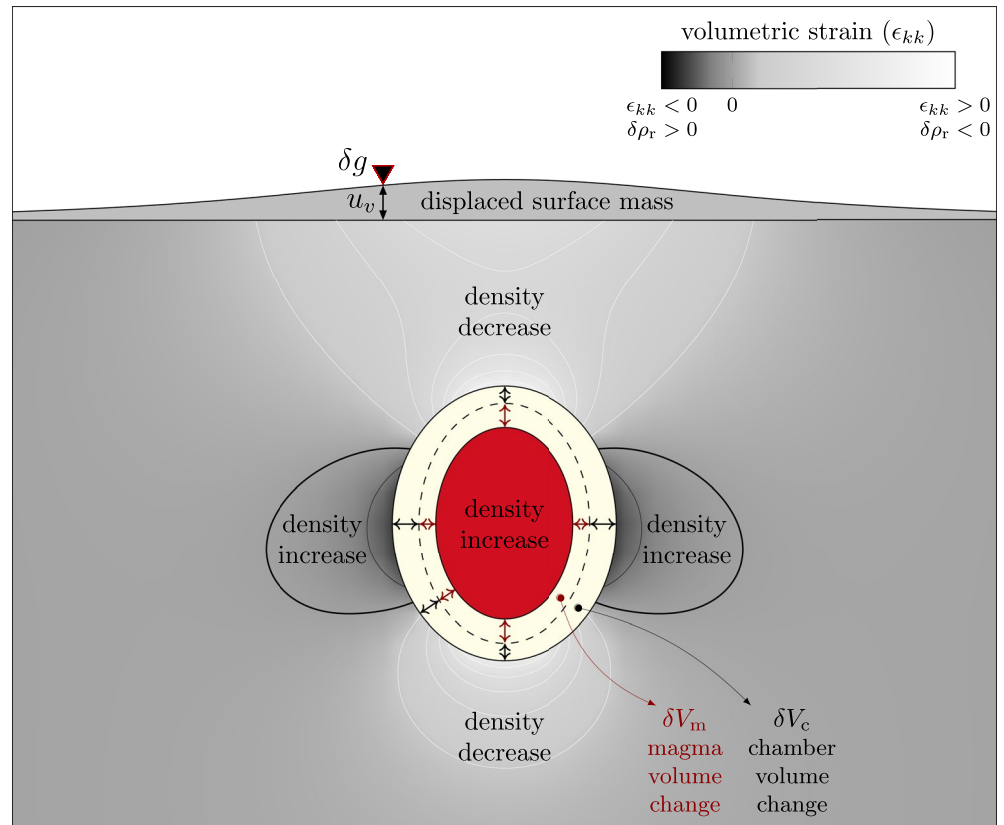
Figure 1. Schematic mass redistribution and surface uplift caused by chamber pressurization. Compressed magma (red) is surrounded by the interface cavity. The dashed ellipse depicts chamber walls prior to pressurization and separates the δV_m and δV_c portions of the interface cavity (see Equation 1). The country rocks are subjected to positive dilatation/density decrease (light gray and white contours) and negative dilatation/density increase (dark gray and black contours). Thick black contour marks zero dilatation. The gravity station (black triangle) has been subjected to gravity change δg and vertical displacement u_v.

In this study, we use the Okubo (1991) expressions to derive analytical solutions for the gravity changes associated with the point CDM. We show how gravity changes due to point and finite ellipsoidal sources can be calculated by using the point CDM. We compare the point CDM gravity changes with the Hagiwara (1977) and Trasatti and Bonafede (2008) solutions. Finally, we elaborate on the potential of the model for coupled inversions of surface displacements and gravity changes.

2. Methods

Deformation-induced gravity changes are usually expressed as the sum of contributions due to deformation in the source region and country rocks and the surface uplift. Here, we adopt a decomposition scheme compatible with the point CDM formulation. We assume a homogeneous, isotropic elastic half-space as a model for the Earth's crust. We denote the Poisson's ratio, shear modulus, and bulk modulus in the medium by ν, μ, and K, respectively. We adopt a right-handed xyz Cartesian coordinate system with the origin at the free surface and the z axis pointing upward. By "gravity change" we refer to the change in the absolute value of the gravity vector's z component. Thus, a positive mass change (mass increase) below a gravimeter leads to a positive gravity change (gravity increase).

2.1. Gravity Changes Caused by Magma Chamber Pressurization

As an example, suppose that magma degassing pressurizes a magma chamber (Figure 1). We assume that the exsolved gases all gather at the interface between the chamber walls and the degassed magma, forming a

shell-shaped cavity. The outward expansion of the chamber walls and inward compression of the magma lead to the oppositely signed chamber volume change, δV_c, and magma volume change, δV_m, respectively. The total volume created by the expansion-compression process—namely the interface volume change, ΔV_{int}—is given by

$$\Delta V_{int} = \delta V_c - \delta V_m, \tag{1}$$

or equivalently by

$$\Delta V_{int} = V_c - V_m, \tag{2}$$

where $V_c = V + \delta V_c$ and $V_m = V + \delta V_m$ are the chamber volume and magma volume in the deformed state, respectively, and V represents both the chamber volume and magma volume in the undeformed state. The chamber expansion also uplifts the surface and generates a strain field, ϵ_{ij}, in the surrounding rocks. This changes the density of the rocks by $\delta \rho_r = -\rho_r \epsilon_{kk}$, where ρ_r is the rock density in the undeformed state and $\epsilon_{kk} = \epsilon_{11} + \epsilon_{22} + \epsilon_{33}$ is the volumetric strain or dilatation—a positive dilatation reduces the density (see Figure 1). Similarly, the magma density change, $\delta \rho_m$, due to the compression is related to the magma compressibility, β_m, through $\delta \rho_m = \rho_m \beta_m \delta p$, where ρ_m is the magma density in the undeformed state and δp is the pressure change in the chamber (Rivalta & Segall, 2008). Provided that β_m and δp are known, we have

$$\delta V_m = V \beta_m \delta p. \tag{3}$$

Since we consider the created volume ΔV_{int} as void, the density change in the δV_c and δV_m portions is $-\rho_r$ and $-\rho_m$, respectively. Similarly, uplift, or subsidence, at the Earth's surface will either fill void space or create a void space. So, the other zone of substantial density change is the Earth's surface, where areas of uplift and subsidence are subjected to density changes $+\rho_r$ and $-\rho_r$, respectively.

The same deformation-induced density changes exist if instead of exsolved gases, the interface cavity is formed by, and filled with, the intrusion of some external fluids. In such case, the interface cavity is filled with a net mass

$$\Delta M = \rho_{int} \Delta V_{int}, \tag{4}$$

where ρ_{int} is the intrusion density.

The magma chamber expansion leads to a vertical displacement, u_v, and the following gravity change contributions for each observation point at the surface:

1. Δg_β, due to density change $\delta \rho_m$ in the magma volume in the deformed state, V_m,
2. $\Delta g_{\delta V_m}$, due to density change $-\rho_m$ within the δV_m volume,
3. $\Delta g_{\delta V_c}$, due to density change $-\rho_r$ within the δV_c volume,
4. $\Delta g_{\epsilon_{kk}}$, due to density changes $\delta \rho_r$ throughout the country rocks,
5. Δg_{SM}, due to the presence of the displaced surface mass layer with density $+\rho_r$,
6. Δg_{FA}, due to the free air change in gravity associated with u_v,
7. $\Delta g_{\Delta M}$, due to the added intrusion mass ΔM that leads to density change ρ_{int} within the interface cavity,

for a total surface gravity change of

$$\delta g = \Delta g_\beta + \Delta g_{\delta V_m} + \Delta g_{\delta V_c} + \Delta g_{\epsilon_{kk}} + \Delta g_{SM} + \Delta g_{FA} + \Delta g_{\Delta M}. \tag{5}$$

$\Delta g_{\Delta M}$, also known as residual gravity, can be used to constrain ΔM (see Battaglia et al., 2008). However, this requires all the other terms in Equation 5 to be quantified first. At each station, δg and u_v can be determined through repeated gravity and deformation measurements, respectively. Then we have

$$\Delta g_{FA} = \gamma u_v, \tag{6}$$

where $\gamma \simeq -0.3086$ mGal/m is the free air gradient, and

$$\Delta g_{SM} = 2\pi G \rho_r u_v, \tag{7}$$

where G is the gravitational constant. Note that Equation 7 uses the Bouguer plate approximation and is valid for flat topographies. The other terms in Equation 5 can be estimated only by using a deformation model for the

chamber pressurization. Note that Equation 5 is valid for sources both in the near field and the far field. In the following, we first introduce an analytical point-source model, which can be applied to sources in the far field, and show that in this case Equation 5 can be simplified. Next, we present a semi-analytical finite-source solution and elaborate on the issues that may limit its applicability to near-field problems.

2.1.1. The Far Field Approximations

The far field gravity changes caused by the intruded fluid mass can be calculated through a point-mass approximation as

$$\Delta g_{\Delta M} = G \Delta M \frac{d}{r^3}, \tag{8}$$

where d is the depth to the center of the chamber and r is the distance between the center of the chamber and the surface observation point. This approximation can also be applied to the far field gravity changes caused by the other density changes in the chamber as

$$\Delta g_\beta = G \delta \rho_m V_m \frac{d}{r^3},$$
$$\Delta g_{\delta V_m} = G \rho_m \delta V_m \frac{d}{r^3},$$
$$\Delta g_{\delta V_c} = -G \rho_r \delta V_c \frac{d}{r^3}, \tag{9}$$
$$\Delta g_{\Delta V_{int}} = -G \rho_r \Delta V_{int} \frac{d}{r^3}.$$

The conservation of the initial magma mass in the chamber implies $\delta \rho_m V_m = -\rho_m \delta V_m$, which together with Equation 9 yields

$$\Delta g_\beta + \Delta g_{\delta V_m} = 0. \tag{10}$$

Note that for shallow finite sources Equation 10 does not necessarily hold, as mass redistribution within the chamber may lead to measurable gravity changes. The far field form of Equation 5 can now be written as

$$\delta g = \Delta g_{\delta V_c} + \Delta g_{\epsilon_{kk}} + \Delta g_{SM} + \Delta g_{FA} + \Delta g_{\Delta M}, \tag{11}$$

which expresses the surface gravity changes associated with a deep pressurized chamber as the sum of contributions due to displaced mass at the chamber walls $\left(\Delta g_{\delta V_c}\right)$, volumetric strain in the host rocks $\left(\Delta g_{\epsilon_{kk}}\right)$, displaced mass at the Earth's surface $\left(\Delta g_{SM}\right)$, and the vertical displacement of gravity stations $\left(\Delta g_{FA}\right)$, superimposed on the mass change contribution $\left(\Delta g_{\Delta M}\right)$.

Note that Equations 1–11 hold for any chamber shape and boundary conditions on the chamber walls.

2.2. Gravity Changes Caused by the Point CDM

The point CDM represents the far field of triaxial sources of expansion with arbitrary spatial orientations (Nikkhoo et al., 2017). The point CDM is composed of three mutually orthogonal point tensile dislocations (see Figure 2a) constrained to either expand or contract together. The strength of each point tensile dislocation is determined by its potency, defined as the product of dislocation surface area and opening (Aki & Richards, 2002; Nikkhoo et al., 2017, see also Appendix A). The point CDM has 10 parameters: three location coordinates, three rotation angles, three potencies specifying the expansion intensity along the three principal axes of the source, and Poisson's ratio, ν. The total potency of the point CDM, denoted by ΔV, is the sum of the three potencies. ΔV has the units of volume but it is not a physical quantity. Rather, it is a measure of the source strength and it holds $\Delta V = \Delta V_{int}$, provided that $K_m = K$, where $K_m = 1/\beta_m$ is the bulk modulus of magma.

Triaxial sources of differing shapes, but identical far field deformation, have the same point CDM representation and thus, the same ΔV. However, in order to have the same δV_c, these sources must also have identical shapes (except for $\nu = 0.5$, which leads to $\Delta V = \delta V_c$). For example, the uniformly pressurized cuboidal and ellipsoidal chambers in Figure 2 have the same potencies but their volume changes are different. Analytical expressions
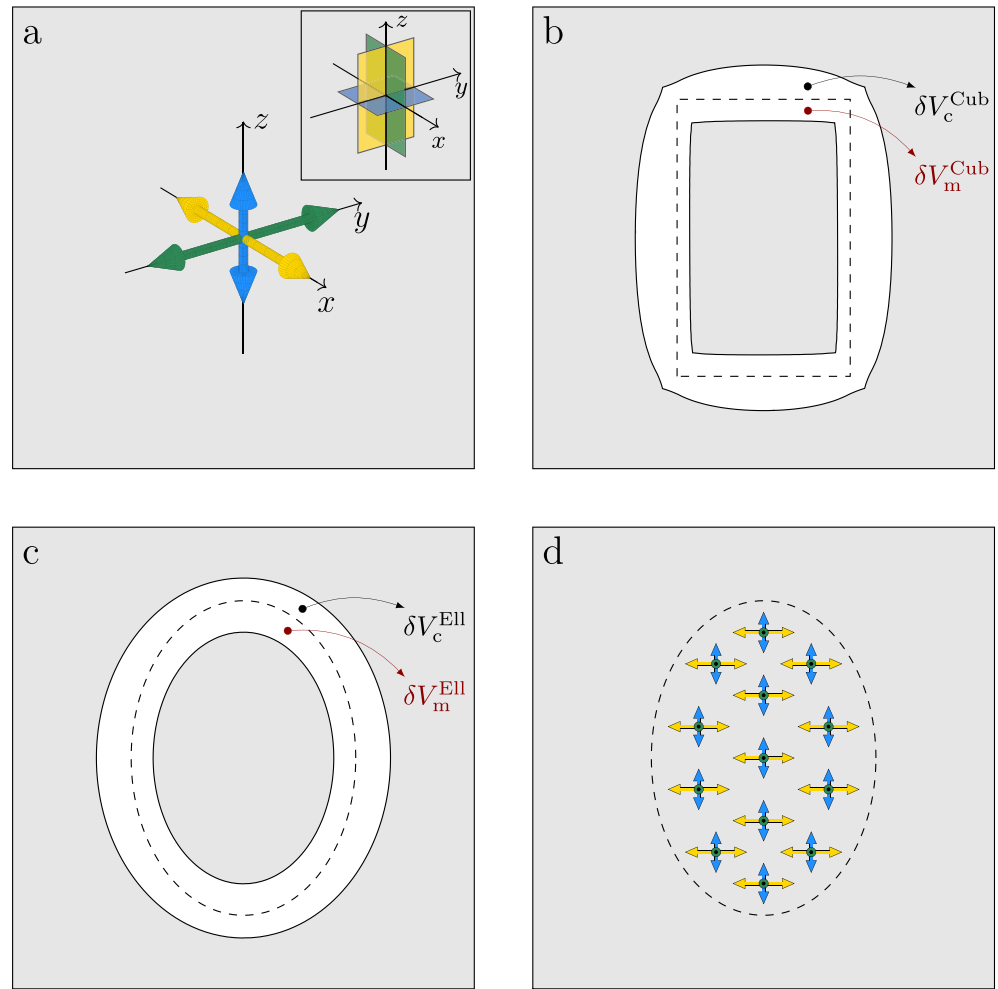
Figure 2. Triaxial volumetric sources. (a) A point Compound Dislocation Model (point CDM) with potencies ΔV_x (yellow), ΔV_y (green), and ΔV_z (blue), where $\Delta V_x = \Delta V_y > \Delta V_z$. Inset shows the equivalent CDM (see Nikkhoo et al., 2017). (b) A uniformly pressurized cuboidal source with $K_m = K$. The two interface cavity portions δV_c^{Cub} and δV_m^{Cub} are indicated, where $\Delta V^{Cub} = \delta V_c^{Cub} + \delta V_m^{Cub}$. (c) Same as (b), but for a uniformly pressurized ellipsoidal source. The interface cavity portions are δV_c^{Ell} and δV_m^{Ell}, with $\Delta V^{Ell} = \delta V_c^{Ell} + \delta V_m^{Ell}$. Note that $\delta V_c^{Cub} \neq \delta V_c^{Ell}$ and $\delta V_m^{Cub} \neq \delta V_m^{Ell}$ but $\Delta V^{Cub} = \Delta V^{Ell}$. (d) A set of N point CDMs uniformly distributed within the ellipsoidal cavity in (c). The point CDM in (a) represents the far field of all the finite sources in (b–d). Provided $N \to \infty$, the near fields of (c and d) are equivalent. For the models in (b and c) $\nu = 0.25$.

relating ΔV to δV_c are available for ellipsoidal sources from Eshelby (1957). For uniformly pressurized ellipsoids, we have (Nikkhoo et al., 2017):

$$\Delta V^{Ell} = \delta V_c^{Ell} + \frac{V \delta p}{K}. \tag{12}$$

Recalling that $K = \frac{2\mu(1+\nu)}{3(1-2\nu)}$ and that for a spherical source of radius a the total volume and volume change are $V^{Sph} = \frac{4}{3}\pi a^3$ and $\delta V_c^{Sph} = \frac{\pi}{\mu}a^3 \delta p$, respectively, Equation 12 becomes

$$\Delta V^{Sph} = \frac{3(1-\nu)}{(1+\nu)} \delta V_c^{Sph}, \tag{13}$$

which for $\nu = 0.25$ leads to $\Delta V^{Sph} = 1.8 \delta V_c^{Sph}$ (see also Aki & Richards, 2002; Bonafede & Ferrari, 2009; Ichihara et al., 2016).

Gravity changes caused by point tensile dislocations can be calculated through the Okubo (1991) analytical expressions (Appendix A). By superimposing the gravity changes associated with three mutually orthogonal point dislocations (Equation A1), we derive the analytical gravity changes associated with the point CDM as

$$\delta g = \Delta g_{\Delta V} + \Delta g_{\mathrm{MD}} + \Delta g_{\mathrm{SM}} + \Delta g_{\mathrm{FA}} + \Delta g_{\Delta M}, \tag{14}$$

where $\Delta g_{\Delta V}$ is the interface cavity contribution (white space in Figures 2b and 2c) and Δg_{MD} is the contribution due to the medium dilatation both inside and outside the source (gray space in Figures 2b and 2c). Noting that $\Delta g_{\Delta V} = \Delta g_{\delta V_{\mathrm{c}}} + \Delta g_{\delta V_{\mathrm{m}}}$ and $\Delta g_{\mathrm{MD}} = \Delta g_{\epsilon_{kk}} + \Delta g_{\beta}$ and using Equation 10 we have

$$\Delta g_{\Delta V} + \Delta g_{\mathrm{MD}} = \Delta g_{\delta V_{\mathrm{c}}} + \Delta g_{\epsilon_{kk}}, \tag{15}$$

from which it follows that the δg from Equation 14 and the δg from Equation 11 are equivalent. Therefore, the point CDM can be used to compute the effects of deformation on gravity change and thus estimate the mass change ΔM.

2.2.1. Gravity Changes Caused by Point and Finite Pressurized Ellipsoidal Cavities

For any point ellipsoidal model after Davis (1986), there is an equivalent point CDM related to the elastic parameters of the medium and the ellipsoid semi-axes and pressure change through the Eshelby (1957) tensor (see Nikkhoo et al., 2017). Thus, Equation 14 also holds for point ellipsoidal sources. By calculating δV_{c} for ellipsoidal cavities $\Delta g_{\delta V_{\mathrm{c}}}$ (Equation 9) and thus, $\Delta g_{\epsilon_{kk}}$ (Equation 15) can be determined for ellipsoidal sources.

Assume that a point CDM with potencies $(\Delta V_a, \Delta V_b, \Delta V_c)$ represents the far field of a pressurized ellipsoidal cavity with semi-axes (a, b, c). Then, a set of N point CDMs with potencies $(\Delta V_a / N, \Delta V_b / N, \Delta V_c / N)$, uniformly distributed within the ellipsoid (see Figure 2d), approximates the near field deformations of the pressurized cavity (Amoruso & Crescentini, 2011; Amoruso et al., 2008; Davis, 1986; Eshelby, 1957; Segall, 2010; Yang et al., 1988). Provided that $N \rightarrow \infty$, this procedure leads to an accurate solution, unless the cavity is immediately below the free surface (Amoruso & Crescentini, 2011; Segall, 2010; Yang et al., 1988). Similar accuracies can be achieved by using the finite Ellipsoidal Cavity Model (finite ECM) after Nikkhoo and Rivalta (2022), which uses a smaller number of point sources with depth-dependent spacing and strengths. By incorporating the expressions for the point CDM gravity changes in these configurations, we derive new solutions for the gravity changes caused by a finite pressurized ellipsoidal cavity. While the finite ECM is more accurate than the point CDM in modeling shallow pressurized ellipsoidal cavities, it is still an approximate solution for both deformation and gravity change calculations. Similar to the Yang et al. (1988) solution, the finite ECM provides excellent accuracies in the limit that the source dimensions are small compared to its depth (see Nikkhoo & Rivalta, 2022, for further details).

3. Results

3.1. Comparisons With Other Gravity Change Solutions

Hagiwara (1977) derived closed-form expressions for the gravity change contributions caused by the Mogi (1958) source, later used to validate analytical (Okubo, 1991) and numerical solutions (Currenti et al., 2007, 2008; Trasatti & Bonafede, 2008).

An isotropic point CDM is equivalent to the Mogi (1958) model (Bonafede & Ferrari, 2009). Assuming potency ΔV^{Sph} and depth d for such a point CDM, Equation A1 yields:

$$\Delta g_{\mathrm{MD}}^{\mathrm{Sph}} = \frac{1}{3} G \rho_{\mathrm{r}} (1 - 2\nu) \Delta V^{\mathrm{Sph}} \frac{d}{r^3},$$

$$\Delta g_{\mathrm{SM}}^{\mathrm{Sph}} = \frac{2}{3} G \rho_{\mathrm{r}} (1 + \nu) \Delta V^{\mathrm{Sph}} \frac{d}{r^3}, \tag{16}$$

$$\Delta g_{\Delta V}^{\mathrm{Sph}} = -G \rho_{\mathrm{r}} \Delta V^{\mathrm{Sph}} \frac{d}{r^3}.$$

By using Equations 9, 13, and 15, we rewrite Equation 16 in terms of $\delta V_{\mathrm{c}}^{\mathrm{Sph}}$:
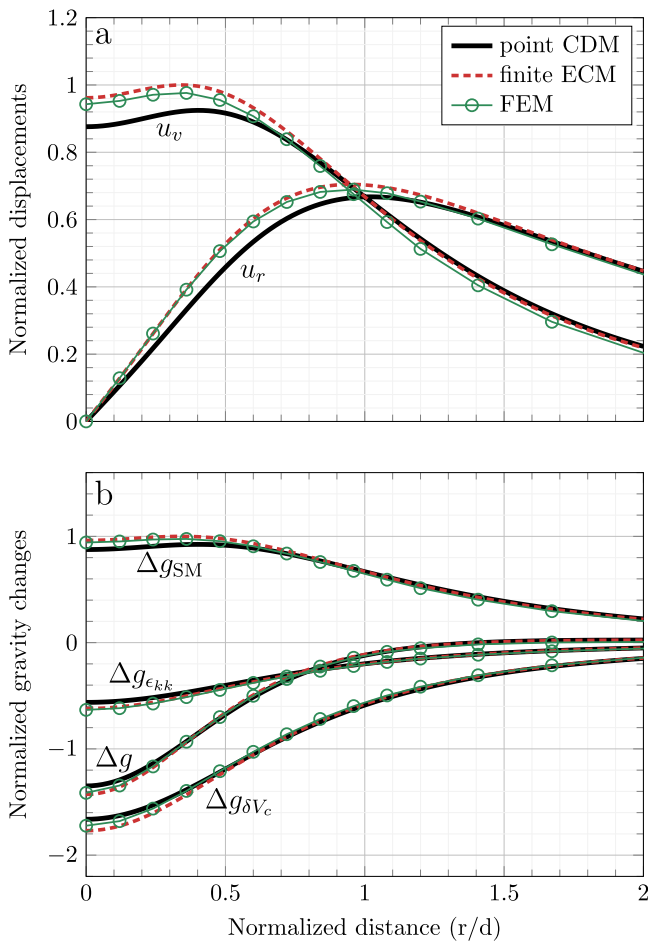
Figure 3. Comparing the finite Ellipsoidal Cavity Model (finite ECM) with the Trasatti and Bonafede (2008) finite element method solution for a vertical prolate spheroidal cavity with semi-major axes 1.842 km, aspect ratio 0.4, and depth to the center 5 km. (a) Radial (u_r) and vertical (u_v) displacements, normalized by the maximum vertical displacement of the finite ECM solution. (b) Gravity change contributions, normalized by the maximum Δg_{SM} of the finite ECM solution.

$$\Delta g_{\epsilon_{kk}}^{\text{Sph}} = -G\rho_r \left(1 - 2\nu\right) \delta V_c^{\text{Sph}} \frac{d}{r^3},$$

$$\Delta g_{\text{SM}}^{\text{Sph}} = 2G\rho_r \left(1 - \nu\right) \delta V_c^{\text{Sph}} \frac{d}{r^3}, \tag{17}$$

$$\Delta g_{\delta V_c}^{\text{Sph}} = -G\rho_r \delta V_c^{\text{Sph}} \frac{d}{r^3},$$

which are equivalent to the Hagiwara (1977) expressions (see also Okubo, 1991; Rundle, 1978; Savage, 1984; Walsh & Rice, 1979). This validates the gravity change solution for the point CDM in the case of point spherical cavities. As proved by Walsh and Rice (1979), the sum of the three terms in each set of Equations 16 and 17 vanishes. Note also that, for any point CDM, if $\nu = 0.5$ then $\Delta g_{\text{MD}} = \Delta g_{\epsilon_{kk}} = 0$.

We now show that the gravity change solutions for the point CDM also provide a basis for rigorous benchmarking of numerical solutions. We use the point CDM and the finite ECM to calculate the surface displacements (Figure 3a) and gravity changes (Figure 3b) associated with the Trasatti and Bonafede (2008) FEM solution for a pressurized vertical prolate spheroidal cavity. In the far field, the point CDM and the finite ECM displacements are indistinguishable. The FEM solution shows a small deviation that can be attributed to the finite domain of the model. In the near field, the finite ECM and FEM displacements show a very good agreement. The maximum ~9% difference between the finite ECM and point CDM reflects the difference between a point-source and a finite-source solution.
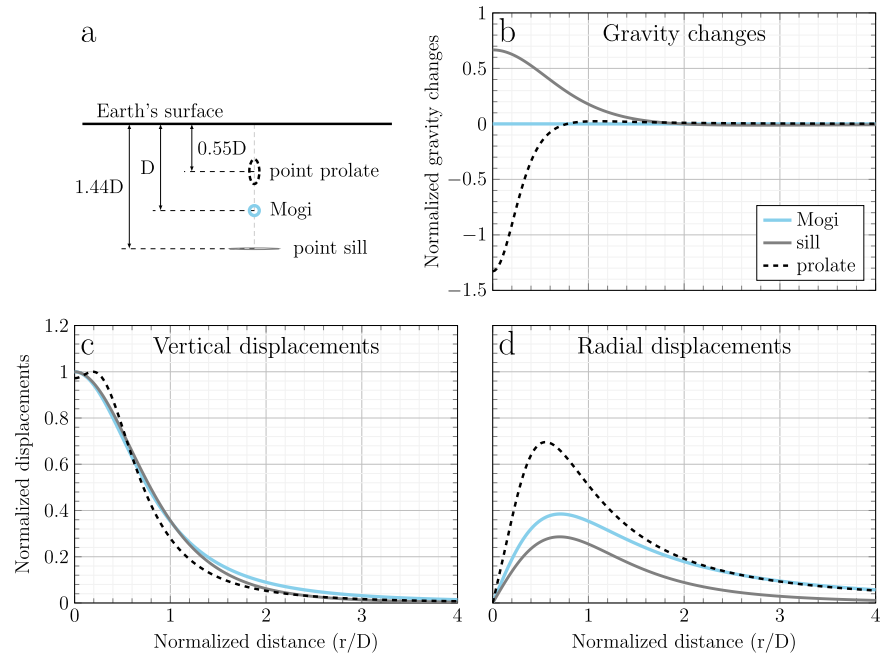
There is also a good agreement between the gravity changes from all approaches (Figure 3b). The maximum differences between $\Delta g_{\delta V_c}$, $\Delta g_{\epsilon_{kk}}$, Δg_{SM}, and Δg from the finite ECM and point CDM are ~6%, ~9%, ~9%, and ~6%, respectively. Since the cavity in this example is relatively deep, the finite ECM calculations are very accurate. Thus, in this particular case, the subtle differences between the finite ECM and the FEM gravity change contributions mostly reflect the errors in the FEM vertical displacements and cavity volume change. The largest difference between the Trasatti and Bonafede (2008) and the other solutions is slightly above 1 μGal, which is more than double the error that Trasatti and Bonafede (2008) estimated by comparison with Hagiwara (1977). This suggests that comparing numerical models with the solution for spherical cavities alone may lead to underestimated errors for the numerical models.

3.2. Implications for the Retrieval of Deformation Source Parameters

Dieterich and Decker (1975) showed that different source shapes produce almost indistinguishable uplift patterns if the source depths are appropriately adjusted. However, the associated horizontal displacements will be completely different. The implication is that in order to constrain all source parameters reliably, horizontal and vertical displacement data must be inverted together. Similar to horizontal and vertical surface displacements, the deformation-induced gravity changes depend on the deformation source parameters. Thus, gravity changes can potentially help better constrain them (Trasatti & Bonafede, 2008).

We use the point CDM to simulate the radial and vertical displacements and the gravity changes associated with three different axially symmetric deformation sources: a horizontal sill, an isotropic source, and a prolate source (see Figure 4). For all sources, $\Delta M = 0$. The source depths in Figure 4a lead to similar vertical displacements (Figure 4c) but distinct horizontal displacements (Figure 4d) and distinct gravity changes (free air contribution removed; Figure 4b). Adjusting the source depths differently (Figure 4e) such that the horizontal displacements match (Figure 4h), leads to distinct vertical displacements (Figure 4f) and distinct gravity changes (Figure 4g). This implies that, from a theoretical perspective, gravity changes may also help to better constrain the deformation
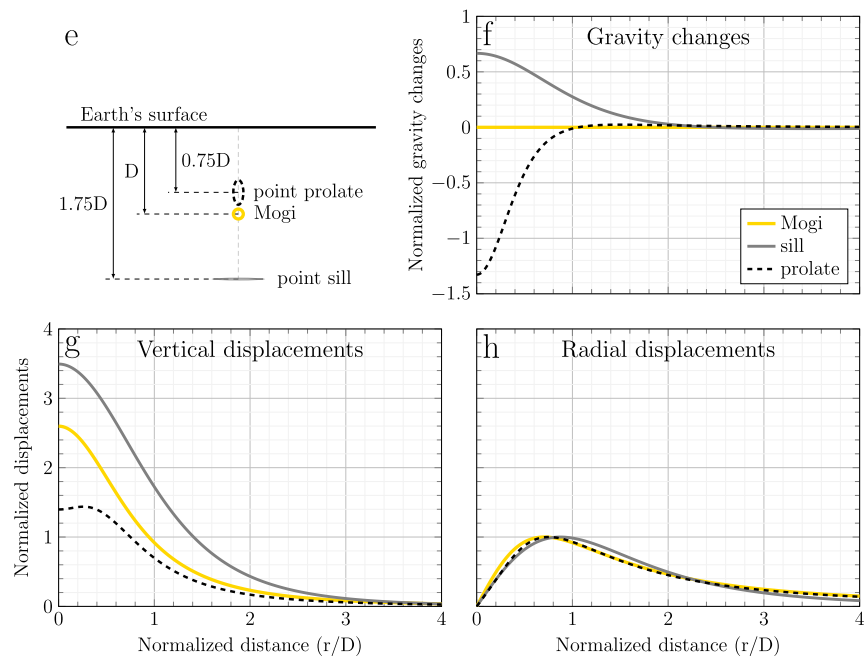
Figure 4. Gravity changes ($\Delta g = \delta g - \Delta g_{FA}$), vertical displacements (u_v), and radial displacements (u_r) for point sources of different aspect ratios and depths. Top block: The sources illustrated in (a) give rise to different Δg (b), similar u_v (c), and different u_r (d). Bottom block: The sources in (e) cause different Δg (f), similar u_r (h), and different u_v (g). The potency vectors of the point spherical source, point prolate source, and point sill in both (a and e) may be any positive multiple of $(1, 1, 1)$, $(1, 1, 0.44)$, and $(0, 0, 1)$, respectively. The gravity changes are normalized by the maximum Δg_{SM} (b and f). The displacements are normalized by the maximum vertical displacement (c and d) and the maximum radial displacements (g and h). All distances are normalized by the depth of the point spherical source, D.

source parameters, beside the mass changes. In practice, however, if $\Delta M \neq 0$, gravity changes may be dominated by $\Delta g_{\Delta M}$ and thus, depending on the signal-to-noise ratio of the data, the Δg curves (Figures 4b and 4f) may become indistinguishable.

4. Discussion

Volcanic gravity changes caused by the net mass of intruding magmatic fluids and the induced host rock deformations may have comparable magnitudes to those of hydrological origin, such as changes in the water table. Such hydrogravimetric disturbances can be estimated by employing hydrological monitoring and modeling techniques (Battaglia et al., 2003, 2006; Creutzfeldt et al., 2010; Kazama et al., 2015; Lien et al., 2014; Van Camp et al., 2010) or by analyzing time-lapse gravity data (Güntner et al., 2017). Thus, the mass of intruding fluids at volcanoes can be inferred reliably once such effects are removed.

New generation, low-cost, and accurate gravimeters might soon provide gravity measurements at an unprecedented spatiotemporal resolution (Carbone et al., 2017, 2020). Permanent networks provide opportunities for new insight on magmatic plumbing systems (Battaglia et al., 2008; Carbone et al., 2019). One main challenge associated with these developments is to perform both detailed Bayesian inferences for in-depth understanding of the volcano, and rapid inversions for hazard assessment and early warning.

The available FEM gravity change models can incorporate various chamber shapes (Currenti, 2014; Currenti et al., 2007, 2008; Trasatti & Bonafede, 2008), the Earth's surface topography (Charco et al., 2009; Currenti et al., 2007), crustal density and material heterogeneities (Currenti et al., 2007, 2008; Trasatti & Bonafede, 2008; Wang et al., 2006), viscoelasticity of the Earth's crust (Currenti, 2018), self-gravitation effects (Charco et al., 2005, 2006; Fernández et al., 2001, 2005), and magma compressibility (Currenti, 2014). Beside difficulties in implementing the FEM, such as meshing issues, this powerful method is computationally too demanding to be used for detailed inverse modeling. In contrast, the point CDM is a half-space model, but has already proven to be suitable for exploring the parameter space in both detailed Bayesian inferences (see Lundgren et al., 2017) and rapid and unsupervised inversions of deformation data (see Beauducel et al., 2020). The gravity change solutions for the point CDM, which we provide here, extend this potential to joint inversions of surface displacements and gravity changes. Volcanic deformation sources are often deep or far enough from the observation point to be treated as far field sources. The point CDM can provide a first order solution, which can be later improved by more sophisticated numerical models. Some complexities such as layering or viscoelasticity can be accounted for (Amoruso et al., 2008) by using appropriate Green's functions for point dislocations (Okubo, 1993; Sun & Okubo, 1993; Wang et al., 2006). Besides, theory errors, arising from ignoring real Earth complexities, can be estimated in terms of noise covariance matrices within a Bayesian framework (see Duputel et al., 2014; Minson et al., 2013; Vasyura-Bathke et al., 2021).

Finite pressurized ellipsoidal cavities can be approximated by a set of point CDMs uniformly distributed in the cavity volumes. With a high number of point CDMs, this approach can be used for benchmarking numerical models. An alternative solution is the finite ECM after Nikkhoo and Rivalta (2022), which provides comparable accuracies for a lesser number of point CDMs. The finite ECM is very fast, and thus, provides a practical way for performing coupled inversions of surface displacements and gravity changes.

It is important to recall that for ellipsoidal deformation models in the half-space, including the finite ECM and the Yang et al. (1988) spheroid, the full-space expressions are used to calculate δV_c (Amoruso & Crescentini, 2009). While this approximation may often be acceptable for deformation studies, it may lead to large errors in gravity change calculations involving shallow finite sources. This warrants future systematic comparisons with numerical models in order to quantify the associated error.

Deformation-induced gravity changes may be substantial (see Figure 3b) and should be accounted for in joint inversions of surface displacements and gravity changes. Provided that coupled models are employed for such inversions, the gravity changes may be exploited to better constrain the deformation source parameters besides the mass change. How practical this may be, depends on the observation uncertainties and the signal-to-noise ratio. We will explore this feature in future studies.

Coupled inversions of surface displacements and gravity changes constrain the deformation source parameters and the intrusion mass without making any assumption on the properties of the intruding fluid. The intrusion

density can be estimated from the inferred mass only if the interface volume change, ΔV_{int}, is known (ΔV_{int} should not be mistaken for the chamber volume change δV_c). It can be shown from Equations 2 and 3 that the determination of ΔV_{int} requires knowledge of the fluid compressibility. This shows that unlike mass change estimates, the estimates of the intrusion density are prone to large uncertainties.

5. Conclusions

1. Surface gravity changes are sensitive to both the intruding fluid mass and the deformation-induced surface uplift (subsidence) and country rock dilatation. Due to this coupling between the gravity changes and host rock deformations, gravity changes can also be used to constrain deformation source parameters, namely the location, spatial orientation, and potency of triaxial source models for expanding reservoirs.
2. We provide analytical solutions and MATLAB codes for surface displacements and gravity changes caused by both the point CDMs, a model for triaxial sources of expansion and the finite ECM, a model for ellipsoidal sources of uniform pressurization.
3. While modeling gravity changes caused by shallow sources, it may be necessary to account for the mass redistribution within the source. This issue and also the inherent error in δV_c for half-space solutions may limit the applicability of the finite ECM.
4. The analytical solutions presented here can be used to validate new numerical gravity change models. Such validations should ideally consider various source depths and aspect ratios.
5. By using the point CDM and the finite ECM, coupled inversions of surface displacements and gravity changes can now be performed.

Appendix A: Gravity Changes Caused by Point Tensile Dislocations

Following the conventions in Section 2 and Okubo (1991), a point tensile dislocation below the origin with depth d, azimuth 0, dip angle θ, potency ΔV, and filled with an intrusion mass ΔM, causes the following gravity change contributions at $(x, y, 0)$

$$
\begin{aligned}
\Delta g_{\Delta V} &= -G\rho_r \Delta V \frac{d}{r^3}, \\
\Delta g_{\text{MD}} &= G\rho_r \Delta V (1 - 2\nu) \left[\frac{d}{r^3} - \frac{1}{r(r+d)} + \frac{x^2(2r+d)}{r^3(r+d)^2} \right] \sin^2\theta, \\
\Delta g_{\text{SM}} &= 2\pi G \rho_r u_v, \\
\Delta g_{\text{FA}} &= \gamma u_v, \\
\Delta g_{\Delta M} &= G\Delta M \frac{d}{r^3},
\end{aligned}
\tag{A1}
$$

where $\Delta g_{\Delta V}$, Δg_{MD}, Δg_{SM}, Δg_{FA}, and $\Delta g_{\Delta M}$ are the contributions due to dislocation cavity, medium dilatation, displaced surface mass, free air effect, and intruded mass, respectively, $r = \left(x^2 + y^2 + d^2 \right)^{1/2}$ and u_v is the surface uplift (see Okada, 1985; Okubo, 1991). Note that for $\nu = 0.5$ and also, for horizontal tensile cracks ($\theta = 0$) we have $\Delta g_{\text{MD}} = 0$.

Data Availability Statement

Data were not used, nor created for this research. The MATLAB codes for computations are available to download at https://volcanodeformation.com/onewebmedia/pCDMgravity.zip. Further details about the dislocation models can be found under https://www.volcanodeformation.com/.

References

Aki, K., & Richards, P. G. (2002). *Quantitative seismology* (2nd ed.). University Science Books.

Amoruso, A., & Crescentini, L. (2009). Shape and volume change of pressurized ellipsoidal cavities from deformation and seismic data. *Journal of Geophysical Research*, *114*(B2), B02210. https://doi.org/10.1029/2008JB005946

Amoruso, A., & Crescentini, L. (2011). Modelling deformation due to a pressurized ellipsoidal cavity, with reference to the Campi Flegrei caldera, Italy. *Geophysical Research Letters*, *38*(1), L01303. https://doi.org/10.1029/2010gl046030

Amoruso, A., & Crescentini, L. (2013). Analytical models of volcanic ellipsoidal expansion sources. *Annals of Geophysics*, *56*(4), 0435. https://doi.org/10.4401/ag-6441

Amoruso, A., Crescentini, L., & Berrino, G. (2008). Simultaneous inversion of deformation and gravity changes in a horizontally layered half-space: Evidences for magma intrusion during the 1982–1984 unrest at Campi Flegrei caldera (Italy). *Earth and Planetary Science Letters*, *272*(1–2), 181–188. https://doi.org/10.1016/j.epsl.2008.04.040

Battaglia, M., Gottsmann, J., Carbone, D., & Fernández, J. (2008). 4D volcano gravimetry. *Geophysics*, *73*(6), WA3–WA18. https://doi.org/10.1190/1.2977792

Battaglia, M., Roberts, C., & Segall, P. (1999). Magma intrusion beneath Long Valley caldera confirmed by temporal changes in gravity. *Science*, *285*(5436), 2119–2122. https://doi.org/10.1126/science.285.5436.2119

Battaglia, M., Segall, P., & Roberts, C. (2003). The mechanics of unrest at Long Valley caldera, California. 2. Constraining the nature of the source using geodetic and micro-gravity data. *Journal of Volcanology and Geothermal Research*, *127*(3–4), 219–245. https://doi.org/10.1016/s0377-0273(03)00171-9

Battaglia, M., Troise, C., Obrizzo, F., Pingue, F., & De Natale, G. (2006). Evidence for fluid migration as the source of deformation at Campi Flegrei caldera (Italy). *Geophysical Research Letters*, *33*(1), L01307. https://doi.org/10.1029/2005gl024904

Beauducel, F., Peltier, A., Villié, A., & Suryanto, W. (2020). Mechanical imaging of a volcano plumbing system from GNSS unsupervised modeling. *Geophysical Research Letters*, *47*(17), e2020GL089419. https://doi.org/10.1029/2020GL089419

Bonafede, M., & Ferrari, C. (2009). Analytical models of deformation and residual gravity changes due to a Mogi source in a viscoelastic medium. *Tectonophysics*, *471*(1–2), 4–13. https://doi.org/10.1016/j.tecto.2008.10.006

Bonafede, M., & Mazzanti, M. (1998). Modelling gravity variations consistent with ground deformation in the Campi Flegrei caldera (Italy). *Journal of Volcanology and Geothermal Research*, *81*(1–2), 137–157. https://doi.org/10.1016/s0377-0273(97)00071-1

Carbone, D., Antoni-Micollier, L., Hammond, G., Zeeuw-van Dalfsen, D., Rivalta, E., Bonadonna, C., et al. (2020). The NEWTON-g gravity imager: Towards new paradigms for terrain gravimetry. *Frontiers in Earth Science*, *8*, 452. https://doi.org/10.3389/feart.2020.573396

Carbone, D., Cannavó, F., Greco, F., Reineman, R., & Warburton, R. J. (2019). The benefits of using a network of superconducting gravimeters to monitor and study active volcanoes. *Journal of Geophysical Research: Solid Earth*, *124*(4), 4035–4050. https://doi.org/10.1029/2018JB017204

Carbone, D., Poland, M. P., Diament, M., & Greco, F. (2017). The added value of time-variable microgravimetry to the understanding of how volcanoes work. *Earth-Science Reviews*, *169*, 146–179. https://doi.org/10.1016/j.earscirev.2017.04.014

Charco, M., Camacho, A. G., Tiampo, K. F., & Fernández, J. (2009). Spatiotemporal gravity changes on volcanoes: Assessing the importance of topography. *Geophysical Research Letters*, *36*(8), L08306. https://doi.org/10.1029/2009gl037160

Charco, M., Fernández, J., Luzón, F., & Rundle, J. (2006). On the relative importance of self-gravitation and elasticity in modeling volcanic ground deformation and gravity changes. *Journal of Geophysical Research*, *111*(B3). https://doi.org/10.1029/2005jb003754

Charco, M., Tiampo, K. F., Luzón, F., & Fernández Torres, J. (2005). Modelling gravity changes and crustal deformation in active volcanic areas. *Física de la Tierra*, *17*, 129–146.

Creutzfeldt, B., Güntner, A., Wziontek, H., & Merz, B. (2010). Reducing local hydrology from high-precision gravity measurements: A lysimeter-based approach. *Geophysical Journal International*, *183*(1), 178–187. https://doi.org/10.1111/j.1365-246x.2010.04742.x

Currenti, G. (2014). Numerical evidence enabling reconciliation gravity and height changes in volcanic areas. *Geophysical Journal International*, *197*(1), 164–173. https://doi.org/10.1093/gji/ggt507

Currenti, G. (2018). Viscoelastic modeling of deformation and gravity changes induced by pressurized magmatic sources. *Journal of Volcanology and Geothermal Research*, *356*, 264–277. https://doi.org/10.1016/j.jvolgeores.2018.03.020

Currenti, G., Del Negro, C., & Ganci, G. (2007). Modelling of ground deformation and gravity fields using finite element method: An application to Etna volcano. *Geophysical Journal International*, *169*(2), 775–786. https://doi.org/10.1111/j.1365-246x.2007.03380.x

Currenti, G., Del Negro, C., & Ganci, G. (2008). Finite element modeling of ground deformation and gravity field at Mt. Etna. *Annals of Geophysics*, *51*(1), 105–119. https://doi.org/10.4401/ag-3037

Davis, P. M. (1986). Surface deformation due to inflation of an arbitrarily oriented triaxial ellipsoidal cavity in an elastic half-space, with reference to Kilauea volcano, Hawaii. *Journal of Geophysical Research*, *91*(B7), 7429–7438. https://doi.org/10.1029/jb091ib07p07429

Dieterich, J. H., & Decker, R. W. (1975). Finite element modeling of surface deformation associated with volcanism. *Journal of Geophysical Research*, *80*(29), 4094–4102. https://doi.org/10.1029/JB080i029p04094

Duputel, Z., Agram, P. S., Simons, M., Minson, S. E., & Beck, J. L. (2014). Accounting for prediction uncertainty when inferring subsurface fault slip. *Geophysical Journal International*, *197*(1), 464–482. https://doi.org/10.1093/gji/ggt517

Eshelby, J. D. (1957). The determination of the elastic field of an ellipsoidal inclusion, and related problems. *Proceedings of the Royal Society of London. Series A. Mathematical and Physical Sciences*, *241*(1226), 376–396. https://doi.org/10.1098/rspa.1957.0133

Fernández, J., Tiampo, K. F., & Rundle, J. B. (2001). Viscoelastic displacement and gravity changes due to point magmatic intrusions in a gravitational layered solid Earth. *Geophysical Journal International*, *146*(1), 155–170. https://doi.org/10.1046/j.0956-540x.2001.01450.x

Fernández, J., Tiampo, K. F., Rundle, J. B., & Jentzsch, G. (2005). On the interpretation of vertical gravity gradients produced by magmatic intrusions. *Journal of Geodynamics*, *39*(5), 475–492. https://doi.org/10.1016/j.jog.2005.04.005

Ferrari, C., Bonafede, M., & Trasatti, E. (2015). Relations between pressurized triaxial cavities and moment tensor distributions. *Annals of Geophysics*, *58*(4), 0438. https://doi.org/10.4401/ag-6737

Güntner, A., Reich, M., Mikolaj, M., Creutzfeldt, B., Schroeder, S., & Wziontek, H. (2017). Landscape-scale water balance monitoring with an iGrav superconducting gravimeter in a field enclosure. *Hydrology and Earth System Sciences*, *21*(6), 3167–3182. https://doi.org/10.5194/hess-21-3167-2017

Hagiwara, Y. (1977). The Mogi model as a possible cause of the crustal uplift in the eastern part of Izu Peninsula and the related gravity change. *Bulletin of the Earthquake Research Institute*, *52*, 301–309.

Ichihara, M., Kusakabe, T., Kame, N., & Kumagai, H. (2016). On volume-source representations based on the representation theorem. *Earth, Planets and Space*, *68*(1), 1–10. https://doi.org/10.1186/s40623-016-0387-3

Kazama, T., Okubo, S., Sugano, T., Matsumoto, S., Sun, W., Tanaka, Y., & Koyama, E. (2015). Absolute gravity change associated with magma mass movement in the conduit of Asama Volcano (Central Japan), revealed by physical modeling of hydrological gravity disturbances. *Journal of Geophysical Research: Solid Earth*, *120*(2), 1263–1287. https://doi.org/10.1002/2014jb011563

Lien, T., Cheng, C.-C., Hwang, C., & Crossley, D. (2014). Assessing active faulting by hydrogeological modeling and superconducting gravimetry: A case study for Hsinchu Fault, Taiwan. *Journal of Geophysical Research: Solid Earth*, *119*(9), 7319–7335. https://doi.org/10.1002/2014JB011285

Lisowski, M. (2007). Analytical volcano deformation source models. In *Volcano deformation: Geodetic monitoring techniques* (pp. 279–304). Springer Berlin Heidelberg. https://doi.org/10.1007/978-3-540-49302-0_8

Lisowski, M., Dzurisin, D., Denlinger, R. P., & Iwatsubo, E. Y. (2008). Analysis of GPS-measured deformation associated with the 2004–2006 dome-building eruption of Mount St. Helens, Washington. In *A volcano rekindled: The renewed eruption of Mount St. Helens, 2004–2006* (Vol. 1750, pp. 301–333). US Geological Survey Reston. https://doi.org/10.3133/pp175015

Lundgren, P., Nikkhoo, M., Samsonov, S. V., Milillo, P., Gil-Cruz, F., & Lazo, J. (2017). Source model for the Copahue volcano magma plumbing system constrained by InSAR surface deformation observations. *Journal of Geophysical Research: Solid Earth*, *122*(7), 5729–5747. https://doi.org/10.1002/2017jb014368

Minson, S., Simons, M., & Beck, J. (2013). Bayesian inversion for finite fault earthquake source models I—Theory and algorithm. *Geophysical Journal International*, *194*(3), 1701–1726. https://doi.org/10.1093/gji/ggt180

Mogi, K. (1958). Relations between the eruptions of various volcanoes and the deformations of the ground surfaces around them. *Bulletin of the Earthquake Research Institute*, *36*, 99–134.

Nikkhoo, M., & Rivalta, E. (2022). Surface deformations caused by pressurized finite ellipsoidal cavities. *Earth and Space Science Open Archive*, *19*. https://doi.org/10.1002/essoar.10510624.1

Nikkhoo, M., Walter, T. R., Lundgren, P. R., & Prats-Iraola, P. (2017). Compound dislocation models (CDMs) for volcano deformation analyses. *Geophysical Journal International*, *208*(2), 877–894. https://doi.org/10.1093/gji/ggw427

Okada, Y. (1985). Surface deformation due to shear and tensile faults in a half-space. *Bulletin of the Seismological Society of America*, *75*(4), 1135–1154. https://doi.org/10.1785/bssa0750041135

Okubo, S. (1991). Potential and gravity changes raised by point dislocations. *Geophysical Journal International*, *105*(3), 573–586. https://doi.org/10.1111/j.1365-246x.1991.tb00797.x

Okubo, S. (1992). Gravity and potential changes due to shear and tensile faults in a half-space. *Journal of Geophysical Research*, *97*(B5), 7137–7144. https://doi.org/10.1029/92jb00178

Okubo, S. (1993). Reciprocity theorem to compute the static deformation due to a point dislocation buried in a spherically symmetric Earth. *Geophysical Journal International*, *115*(3), 921–928. https://doi.org/10.1111/j.1365-246x.1993.tb01501.x

Okubo, S., Hirata, Y., Sawada, M., & Nagasawa, K. (1991). Gravity change caused by the 1989 earthquake swarm and submarine eruption off Ito, Japan test on the magma intrusion hypothesis. *Journal of Physics of the Earth*, *39*(1), 219–230. https://doi.org/10.4294/jpe1952.39.219

Rivalta, E., & Segall, P. (2008). Magma compressibility and the missing source for some dike intrusions. *Geophysical Research Letters*, *35*(4), L04306. https://doi.org/10.1029/2007gl032521

Rundle, J. B. (1978). Gravity changes and the Palmdale uplift. *Geophysical Research Letters*, *5*(1), 41–44. https://doi.org/10.1029/gl005i001p00041

Savage, J. (1984). Local gravity anomalies produced by dislocation sources. *Journal of Geophysical Research*, *89*(B3), 1945–1952. https://doi.org/10.1029/jb089ib03p01945

Segall, P. (2010). *Earthquake and volcano deformation*. Princeton University Press.

Sun, W., & Okubo, S. (1993). Surface potential and gravity changes due to internal dislocations in a spherical Earth—I. Theory for a point dislocation. *Geophysical Journal International*, *114*(3), 569–592. https://doi.org/10.1111/j.1365-246x.1993.tb06988.x

Trasatti, E., & Bonafede, M. (2008). Gravity changes due to overpressure sources in 3D heterogeneous media: Application to Campi Flegrei caldera, Italy. *Annals of Geophysics*, *51*, 121–135. https://doi.org/10.4401/ag-4442

Van Camp, M., Métivier, L., De Viron, O., Meurers, B., & Williams, S. (2010). Characterizing long-time scale hydrological effects on gravity for improved distinction of tectonic signals. *Journal of Geophysical Research*, *115*(B7), B07407. https://doi.org/10.1029/2009jb006615

Vasyura-Bathke, H., Dettmer, J., Dutta, R., Mai, P. M., & Jonsson, S. (2021). Accounting for theory errors with empirical Bayesian noise models in nonlinear centroid moment tensor estimation. *Geophysical Journal International*, *225*(2), 1412–1431. https://doi.org/10.1093/gji/ggab034

Walsh, J., & Rice, J. (1979). Local changes in gravity resulting from deformation. *Journal of Geophysical Research*, *84*(B1), 165–170. https://doi.org/10.1029/jb084ib01p00165

Wang, R., Lorenzo-Martin, F., & Roth, F. (2006). PSGRN/PSCMP—A new code for calculating co-and post-seismic deformation, geoid and gravity changes based on the viscoelastic-gravitational dislocation theory. *Computers & Geosciences*, *32*(4), 527–541. https://doi.org/10.1016/j.cageo.2005.08.006

Yang, X.-M., Davis, P. M., & Dieterich, J. H. (1988). Deformation from inflation of a dipping finite prolate spheroid in an elastic half-space as a model for volcanic stressing. *Journal of Geophysical Research*, *93*(B5), 4249–4257. https://doi.org/10.1029/JB093iB05p04249